Journal of Applied Polymer Science

Preparation, Characterization, and Adsorption Performance of p-Hydroxybenzoic Acid Imprinted Polymer and Selective Catalysis of Toluene to *para*-Chlorotoluene

Minjia Meng,[1] Lanlan Bao,[1] Minqiang He,[1] Kaiyong Sun,[1] Weibing Li,[1] Dexiang Zhao,[1] Yonghai Feng,[2] Yongsheng Yan[1]

[1]School of Chemistry and Chemical Engineering, Jiangsu University, Zhenjiang 212013, China
[2]School of Materials Science and Engineering, Jiangsu University, Zhenjiang 212013, China
Correspondence to: M. He (E-mail: hemq@ujs.edu.cn)

ABSTRACT: A *p*-hydroxybenzoic acid surface molecularly imprinted polymer (*p*-HB–**S**MIP) with **si**lica microspheres as a supporting matrix was prepared by the adoption of the surface molecular imprinting technique with acrylamide (**AM**) as a functional monomer, ethylene glycol dimethacrylate as a crosslinker, and azoisobutyronitrile as an initiator. The *p*-HB–SMIP was characterized by scanning electron microscopy, Fourier transform infrared spectroscopy, and thermogravimetry. Interactions between the functional monomer and template were observed with UV–visible spectroscopy of the solutions of these components as well. The results indicate that a 1:2 molecular complex was formed between *p*-hydroxybenzoic acid (*p*-HB) and AM. A kinetic binding study showed that *p*-HB–SMIP reached saturation adsorption after about 1 h, and the pseudo-second-order model fitted the adsorption kinetics data. Static adsorption experiments revealed that the Freundlich equation fitted the adsorption isotherm data. The thermodynamics parameters (with positive values of enthalpy and entropy and negative values of Gibbs free energy) indicated that the binding system for *p*-HB–SMIP was endothermic and entropy was gained and was spontaneous. Selective experiments showed that *p*-HB–SMIP had a high affinity and excellent recognition selectivity for the template *p*-HB. *p*-HB–SMIP was further investigated by the catalysis of toluene to *para*-chlorotoluene. The catalytic reaction results showed that the conversion of toluene was 85.5% and the molar ratio of *para*-chlorotoluene to *o*-chorotoluene was 1.38; this was higher than that of traditional catalysts. © 2013 Wiley Periodicals, Inc. J. Appl. Polym. Sci. **2014**, *131*, 40118.

KEYWORDS: molecularly imprinted polymer; p-hydroxybenzoic acid; selectivity; *para*-chlorotoluene; catalysis

Received 29 August 2013; accepted 24 October 2013
DOI: 10.1002/app.40118

INTRODUCTION

para-Chlorotoluene is a very important intermediate, which has been widely used in the manufacturing of dyes, pharmaceuticals, and pesticides. In industry, *para*-chlorotoluene is obtained by the reaction of the chlorination of toluene, which is an electrophilic substitution process that occurs at the ortho and para positions.[1] Homogeneous Lewis acid catalysts such as $FeCl_3$, $AlCl_3$, and $SbCl_3$ are typically used for the chlorination of toluene, and the products are produced in *para*-chlorotoluene/*ortho*-chlorotoluene isomer ratios (*p*/*o*) on the order of 0.5.[2] However, *para*-chlorotoluene is more valuable than *ortho*-chlorotoluene on the market. Furthermore, a large amount of water may be added to the reaction mixture to neutralize the Lewis acid catalyst and separate it from the chlorinated products. The catalyst cannot be economically recovered after this step, and consequently, aqueous waste is generated. Consequently, new efficient catalysts should be developed to increase the selectivity of *para*-chlorotoluene and to obtain a high recovery.

Molecular imprinting technology is a promising method for the design of molecularly imprinted polymers (MIPs). It allows the creation of artificial recognition sites with the target analyte (the template molecule).[3–5] Host structures are obtained by the self-assembly of functional monomers with the template molecule. After polymerization, the template is removed, and a free cavity is obtained with a shape and an arrangement of functional groups that are complementary to the structure of the template. Traditionally, because of the thick polymeric network, most MIPs was prepared by bulky polymerization with poor site accessibility to the target molecules and a low rebinding capacity.[6,7] To effectively overcome these drawbacks, the surface molecular imprinting technique has been developed to provide binding sites on the surface of support with more accessible

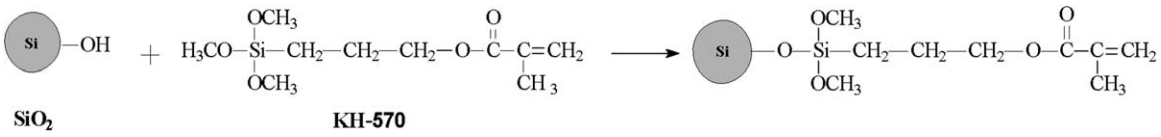

Scheme 1. Silanization of AS by KH-570.

sites and to ensure fast binding kinetics. In addition, the chemical and physical stabilities of MIPs, including their compatibility with organic solvents and tolerance to a wide range of pHs and temperatures, have led to their use as affinity matrices in many analytic application areas,[8–15] and they have also been applied to the preparation of shape-selective catalysts.[16–24]

A promising though challenging field for the application of MIP technology is organic synthesis and, in particular, catalysis. Although a growing number of catalysis have been designed and synthesized for a number of different reaction types (e.g., ester hydrolysis,[25] transamination,[26] β-elimination),[27] only a few studies have dealt with the chlorination of an alkyl aromatic such as toluene.

In this study, we introduced a catalytic imprinted polymer, which was prepared by the imprinting of a product analogue [*p*-hydroxybenzoic acid (*p*-HB)] through complex formation between a functional monomer and the product analogue template molecule. The adsorption properties and capacity were demonstrated by static binding experiments and the thermodynamics parameters. Finally, the catalytic activity for the chlorination of toluene was evaluated through the *p*/*o* values.

EXPERIMENTAL

Materials

Silica particles (0.5–2 μm) were purchased from Nanjing Haitai Nanomaterial Co., Ltd. (Nanjing, Jiangsu, China). 3-Methacryloxypropyltrimethoxysilane (KH-570) was obtained from Jiangsu Chenguang Co., Ltd. (Zhenjiang, Jiangsu, China). *p*-HB, salicylic acid (SA), *p*-aminobenzoic acid (*p*-ABA), toluene, benzoic acid (BA), acetonitrile, and acrylamide (AM) were all supplied by Sinopharm Chemical Reagent Co., Ltd. Ethylene glycol dimethacrylate (EDMA) was purchased from Shanghai Haiqu Chemical Co., Ltd. (Shanghai, China). 2,2′-Azobisisobutyronitrile (AIBN) was purchased from Shanghai No. 4 Reagent & H. V. Chemical Co., Ltd. (Shanghai, China). EDMA was distilled *in vacuo* before use. AIBN was purified by recrystallization from ethanol. All chemicals were analytical-reagent grade, except for methanol, which was high-performance liquid chromatography (HPLC) grade.

Spectrophotometric Analysis of the Template–Monomer Interaction

Ultraviolet–visible (UV–vis) spectrophotometric analysis was performed to characterize the stability of the complexes formed between *p*-HB and the functional monomers in the solution before polymerization. A series of solutions was prepared with a constant concentration of *p*-HB (0.05 mmol/L) and various amounts of AM in acetonitrile. The change in absorption (ΔA) of these solutions was determined at 251 nm with corresponding acetonitrile solutions of AM as references. The average data of triplicate independent experiments were used for the plots of $\Delta A/b_0$ (where b_0 is the AM analytic concentration) versus ΔA, as described in literature.[28,29]

Preparation of the Surface MIP

Activation of Silica. An amount of 20 g of silica was added to 150 mL of a solution of 5% HNO_3 in a flask. Then, the mixture was refluxed at 80°C for 24 h under vigorous magnetic stirring, filtered, and washed with distilled water several times to remove residual HNO_3. Subsequently, the activated silica (AS) was dried at 60°C *in vacuo* for silanization.

Silanization of AS. C═C bond was introduced onto the surface of AS by silanization with the coupling agent KH-570, as shown in Scheme 1.

Dried AS (10 g) was dispersed in absolutely dry toluene (100 mL) in a three-necked, round-bottomed flask under a nitrogen atmosphere with continuous stirring. The coupling agent KH-570 (7.5 g) and triethylamine (1 mL) were added to the flask, and the reaction was carried out at 70°C for 24 h under magnetic stirring. KH-570 was grafted onto silica particles surface in a coupling manner. The product particles were separated from the mixture via centrifugation and washed with toluene, acetone, and methanol, respectively. Finally, the silanized silica was gained by *in vacuo* drying at 80°C for 24 h.

Procedures for the Preparation of the *p*-HB Surface Molecularly Imprinted Polymer (*p*-HB–SMIP). The schematic illustration of the synthetic route for *p*-HB–SMIP is displayed in Figure 1. The template *p*-HB (1 mmol) and the functional monomer AM (4 mmol) were dissolved in acetonitrile (15 mL) in a glass vial (50 mL). After being shaken for 6 h, silanized silica (2.55 g), the crosslinking agent EDMA (20 mmol), and the initiator AIBN (34 mg) were added. The mixture was fully stirred for 4 h at room temperature; this was followed by thorough purging with nitrogen for 10 min, and the mixture was then sealed *in vacuo*. The polymerization was started by thermal initiation in a water bath at 60°C for 24 h. The product particles were washed repeatedly with a mixed solvent of methanol and acetic acid (9:1 v/v) to remove the template and the remaining monomer. Finally, *p*-HB–SMIP was obtained by filtration and drying. As a contrast, the surface nonimprinted material (SNIP) was prepared in the absence of the template and treated with the same method.

Characterization

The morphology and structure of the products were characterized by scanning electron microscopy (SEM; S-4800) with Fourier transformation infrared (FTIR) spectroscopy (Nicolet NEXUS-470 FTIR instrument), thermogravimetry (TG; Netzsch STA-449C), and HPLC (Shimadzu, Japan), with an instrument equipped with a UV detector for the detection of the analogues (*p*-HB, SA, *p*-ABA, and BA). The injection loop volume was 5 μL, and the mobile phase consisted of 1% acetic acid and

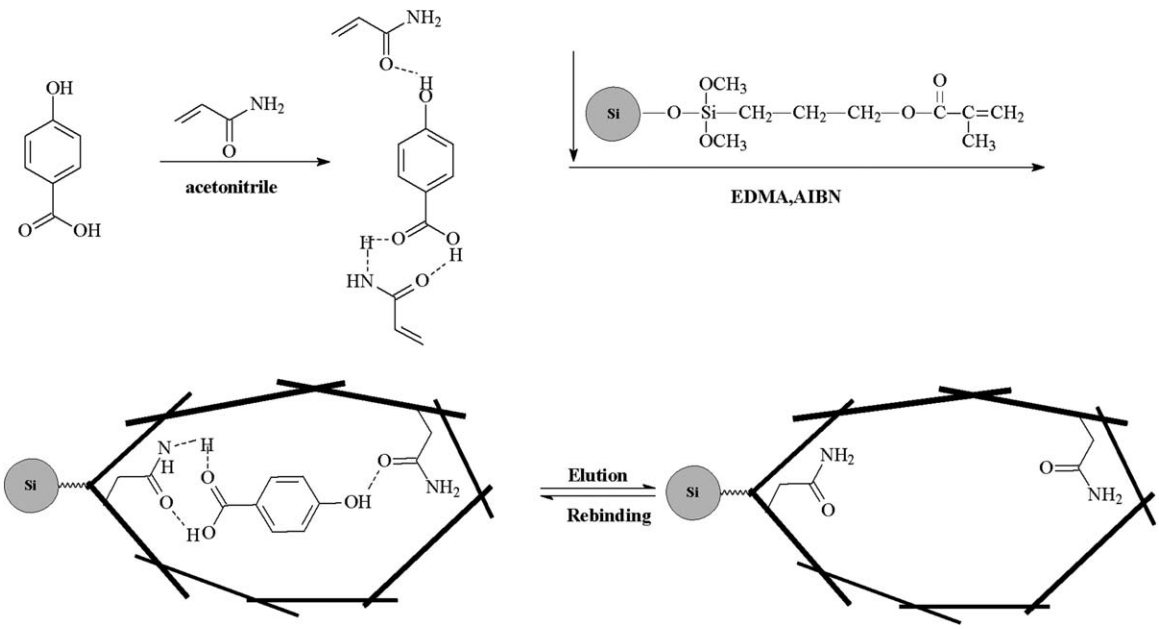

Figure 1. Synthetic route of *p*-HB–SMIP.

methanol with a volume ratio of 50:50. The flow rate of the mobile phase was 1.0 mL/min. The oven temperature was set at 25°C, and then, *p*-HB, SA, *p*-ABA, and BA were all detected at 250 nm.

Batch Mode Adsorption Experiments

The adsorption kinetics process of *p*-HB on *p*-HB–SMIP was studied at room temperature. An amount of 0.01 g of *p*-HB–SMIP was put into a conical flask containing 10 mL of *p*-HB solution (1.5 mmol/L). The mixture was shaken in a constant-temperature shaker for different time periods (0–5 h) and then centrifuged at 20,000 rpm for 3 min. After adsorption, the concentration of *p*-HB in the mixed solution was determined with UV–vis spectroscopy at a wavelength of 251 nm. The *binding amount,* which was defined as the micromoles of the template molecule *p*-HB bound per gram of polymer, was calculated with eq. (1). The curve of the binding amount versus time was plotted, and the time in which the adsorption reached equilibrium was determined:

$$Q = \frac{(C_0 - C_t)V}{W} \quad (1)$$

where Q is the binding amount of *p*-HB on *p*-HB–SMIP (μmol/g), C_0 is the initial concentration of *p*-HB (mmol/L), C_t is the concentration of *p*-HB at time t (mmol/L), and V and W are the volume of the solution (L) and the mass of the adsorbent *p*-HB–SMIP (g), respectively.

The adsorption isotherm of *p*-HB was obtained at room temperature by the addition 0.05 g of *p*-HB–SMIP or SNIP into 3 mL of *p*-HB solution with the initial concentrations of *p*-HB in acetonitrile. After 6 h of shaking, *p*-HB and SMIP were separated by centrifugation at 20,000 rpm for 3 min, and the concentration of *p*-HB in the mixed solution was determined with UV–vis absorption spectroscopy at a wavelength of 251 nm. The equilibrium binding amounts were calculated with eq. (2).

$$Q = \frac{(C_0 - C)V}{W} \quad (2)$$

where C is the equilibrium concentration of *p*-HB (mmol/L).

The binding parameters of *p*-HB–SMIP were mainly estimated by Scatchard analysis with the data from the static binding experiment. The Scatchard equation is presented in eq. (3):

$$\frac{Q}{C} = \frac{(Q_{max} - Q)}{K_d} \quad (3)$$

where Q is the equilibrium binding amount of *p*-HB on *p*-HB–SMIP (μmol/g), Q_{max} is the apparent maximum binding amount (μmol/g), and K_d is the equilibrium dissociation constant (μmol/mL).

Selective Recognition Experiments

To measure the selective recognition of *p*-HB–SMIP for *p*-HB, SA, *p*-ABA, and BA were selected as competitive compounds. The sizes and structures of the three substances were similar to those of *p*-HB to a certain extent. The molecular structures of the three substances are shown schematically in Figure 2.

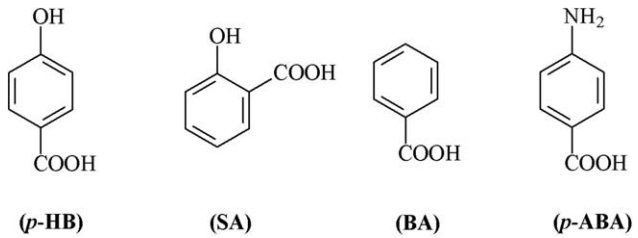

Figure 2. Structures of *p*-HB, SA, BA, and *p*-ABA.

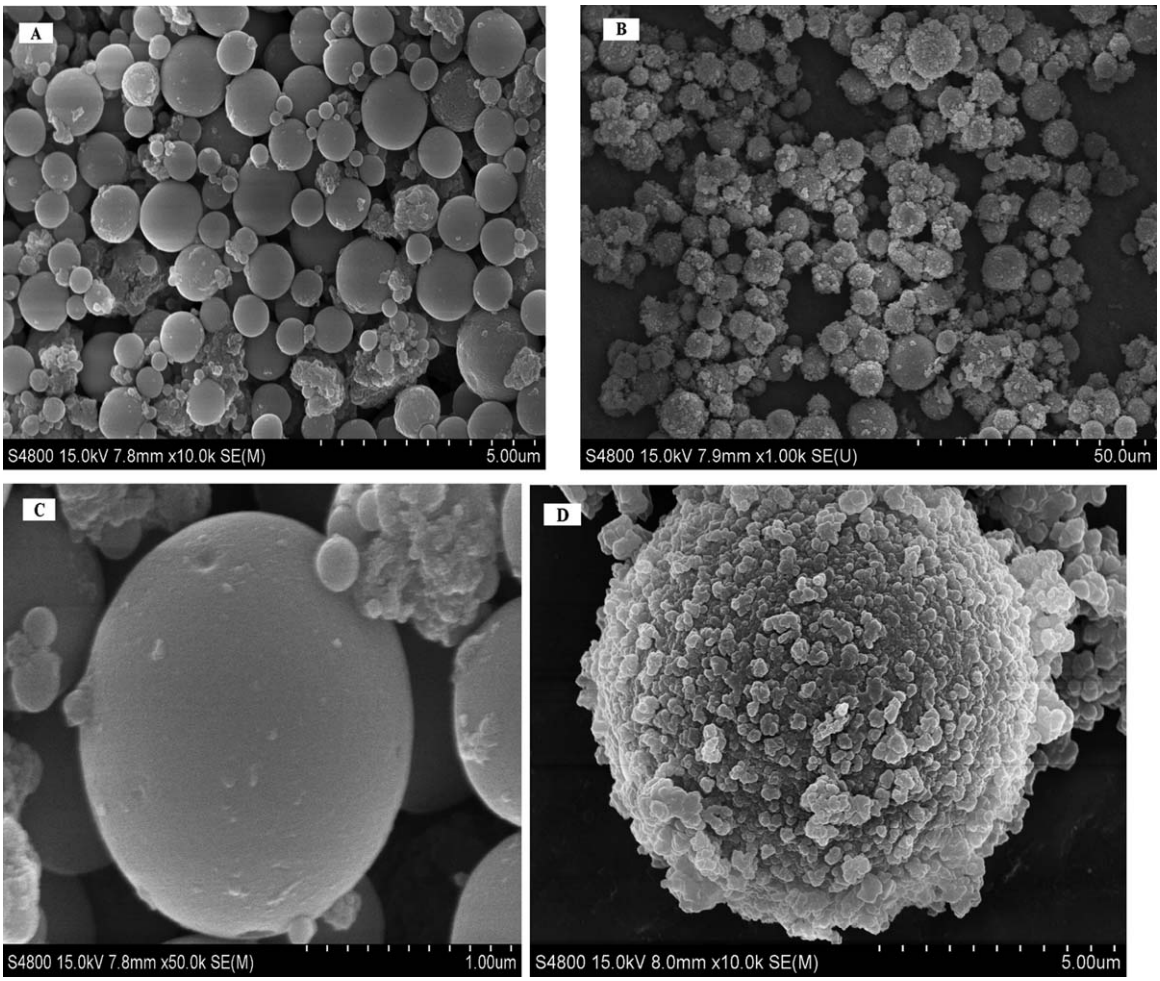

Figure 3. SEM images of (A,C) AS and (B,D) *p*-HB–SMIP.

During the experiment, the coexisting compound solution (*p*-HB, SA, *p*-ABA, and BA), in which the concentration of each compound was 8.0 μmol/mL, was treated according to the procedure of batch mode adsorption studies. Then, the concentration of *p*-HB in the solvent phase was determined with HPLC. The distribution coefficient (K_d), selectivity coefficient (α), and relative selectivity coefficient (α') values of *p*-HB, SA, *p*-ABA, and BA were obtained with eqs. (4)–(6):

$$K_d = \frac{C}{C_e} \tag{4}$$

where C_e is the equilibrium concentration of each *p*-HB analogue in solution (mmol/L). α for the binding of the specific *p*-HB analogues was obtained according to the following equation:

$$\alpha = \frac{KD_i}{KD_j} \tag{5}$$

where *i* and *j* represent the template and competition species, respectively. The value of α allowed us to estimate the selectivity of *p*-HB–SMIP for *p*-HB. α' is defined in eq. (6), and the value of α' indicated the enhanced extent of adsorption affinity and the selectivity of the imprinted material for the template molecule relative to SNIP:

$$\alpha' = \frac{\alpha_M}{\alpha_N} \tag{6}$$

where α_M is the selectivity coefficient of *p*-HB–SMIP for *p*-HB relative to the competition species and α_N is the selectivity coefficient of SNIP for *p*-HB relative to the same competition species.

Catalytic Chlorination of Toluene

The chlorination of toluene was carried out in a 100-mL three-necked flask with a magnetic stirring. An amount of 0.5 g of *p*-HB–SMIP was added to 20 mL of acetonitrile in the flask. To the mixture were added 10 mL of toluene and 7.5 mL of sulfuryl chloride with vigorous stirring with a water bath. The reaction was carried out at a temperature of 60°C for a reaction time of 60 min. The collected reaction products were analyzed on a gas chromatograph equipped with flame ionization detector (FID) and an OV-1701 packed capillary column (0.25 mm × 30 m).

The conversion of toluene and the selectivity of products were the factors that we used to evaluate the catalyst performance. They were defined by the following equations:

$$\text{Conversion (\%)} = \text{Amount of converted toluene (mol)} / \text{Total amount of toluene (mol)} \times 100$$

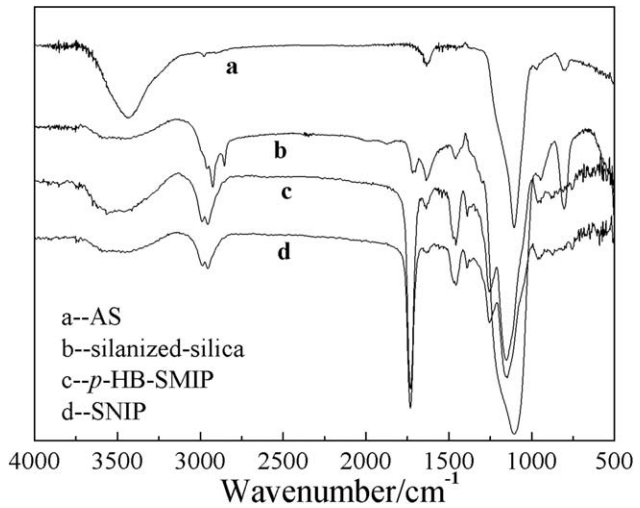

Figure 4. FTIR spectra of (a) AS, (b) silanized silica, (c) *p*-HB–SMIP, and (d) SNIP.

$$\text{Selectivity (\%)} = \text{Amount of one product (mol)} / \text{Amount of all of the products (mol)} \times 100$$

RESULTS AND DISCUSSION

Characteristics of *p*-HB–SMIP

SEM was used to capture the detailed morphologies of AS and *p*-HB–SMIP. Figure 3 shows the SEM images of AS [Figure 3(A)] and *p*-HB–SMIP [Figure 3(B)]. Figure 3(C,D) presents the corresponding magnified figures of AS and *p*-HB–SMIP, respectively. We observed that AS was well dispersed in a spherical shape with bare surfaces and *p*-HB–SMIP retained homogeneous spheres. Compared with AS, the surface of *p*-HB–SMIP was rough and ruleless; this was the result of coating by the products from the crosslinking reaction.

The FTIR spectra of AS, silanized silica, *p*-HB–SMIP, and SNIP were measured and are shown in Figure 4(a–d). Compared with AS, we found that the new absorption peaks at 2960 and 1711 cm^{-1} in the spectrum of silanized silica were due to the stretching vibration absorptions of the saturated C—H band and carbonyl C=O in the ester groups, respectively. These results suggest that KH-570 was successfully grafted onto the surface of SiO_2 (AS). At the same time, in the spectrum of silanized silica, there were weakened bands at about 3433 cm^{-1}; this was the vibration absorption peak of the O—H bond groups. Compared with that of silanized silica, the spectra of the imprinted and nonimprinted materials showed that the stretching vibration absorption of the saturated C—H band and carbonyl C=O in the ester groups were distinctly strengthened; this resulted from the polymerization crosslinking process. The IR data proved that the surface-imprinted polymer *p*-HB–SMIP was obtained.

On the basis of the different thermal stabilities among AS, silanized silica, and *p*-HB–SMIP, the grafting amount and imprinting layer content of *p*-HB–SMIP on the surface of AS was measured by TG analysis. Figure 5 shows the TG curves of the AS, silanized silica, and *p*-HB–SMIP, respectively; this suggested that the *p*-HB–SMIP had good thermal stability.

The AS was stable without evident weight loss below 500°C. The silanized silica exhibited a slight weight loss of about 16.36% from room temperature to 500°C; this was mainly due to the loss of an amount of grafting polymer during the silanization. However, *p*-HB–SMIP was stable to 300°C; beyond this temperature, the polymer degraded until it reached 450°C, with a larger weight loss of about 70%. The difference in the weight loss in this range between *p*-HB–SMIP and the original AS indicated that the polymer grafted to AS accounted for about 68% of the total weight of *p*-HB–SMIP.

Interaction Between the Template and the Functional Monomers

It was of obvious importance that the functional monomers interacted strongly with the template and formed stable host–guest complexes before polymerization.[30]

The complexes formed between the print molecule and the functional monomers can be generally expressed as follows:

$$T + nM \overset{K}{\rightleftharpoons} TM_n$$

where T is template molecule, M is the functional monomer, K is the association constant and n refers to the composition of complex (n=5 1, 2, 3, …, q).

To study the stability of complexes formed between a template and functional monomers, a spectroscopic method is often used.[29]

In theory, for a b_0 greater than the analytic concentration of *p*-HB (a_0), the complex concentration (c) can be calculated as follows:

$$c = \frac{a_0 b_0^n K}{1 + b_0^n K} \tag{7}$$

$$A + nB = C \tag{8}$$

where A and B represent template molecule and functional monomer, respectively. The absorbance measured at a wavelength where B does not absorb is

$$A = [(a_0 - c)\varepsilon_A + c\varepsilon_C]l \tag{9}$$

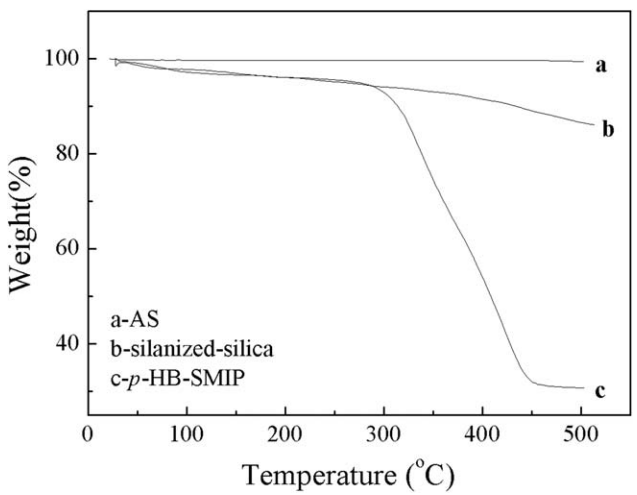

Figure 5. TG curves of AS, silanized silica, and *p*-HB–SMIP.

where l is optical distance, ε_A and ε_C are the molar absorptivities of A and C, respectively. For $b_0 = 0$, the absorbance is

$$A_0 = a_0 \varepsilon_A l \tag{10}$$

Where A_0 is the absorbance of template molecule (A) at the concentration of a_0. The absorbance difference measured is

$$\Delta A = A - A_0 = c \Delta \varepsilon l \tag{11}$$

where $\Delta\varepsilon$ is the difference between the molar absorptivities of A and C. The substitution of eq. (11) into eq. (7) yields

$$\frac{\Delta A}{b_0^n} = -K\Delta A + K\Delta\varepsilon_C a_0 l \tag{12}$$

where we obtained K and n by plotting $\Delta A/{b_0}^n$ versus ΔA. Where b_0 is the concentration of functional monomer, n represents stoichiometric ratio in equation 8.

As shown in Figure 6, only when $n = 2$ was the plot of $\Delta A/{b_0}^n$ versus ΔA linear [correlation coefficient $(R^2) = 0.997$]. K was calculated from its slope to be $4.993 \times 10^6\ M^{-2}$. This indicated that the 1:2 complex may have been predominant in the prepolymerization mixture.

Adsorption Kinetics

The adsorption kinetic curves of *p*-HB–SMIP for the template *p*-HB are given in Figure 7. As shown in this figure, the adsorption amounts of *p*-HB on *p*-HB–SMIP increased quickly with time during the first 50 min, and then, the adsorption amounts increased slowly with time. About 100 min later, the adsorption process reached equilibrium. It was reasonable to assume that a large number of imprinted cavities existed on the surface of the imprinting material, so it was easier for the template *p*-HB to enter into the cavities and bind with the recognition sites. With the template *p*-HB filling up the recognition sites on the surface of *p*-HB–SMIP, the molecules hardly entered the cavities and bound with the recognition sites because of the diffusion resistance; this caused a gradual decrease in the adsorption rates. In this study, the fast adsorption process indicated that the diffusion resistance for *p*-HB was smaller, and the *p*-HB–SMIP had good site accessibility and mass transport for *p*-HB.

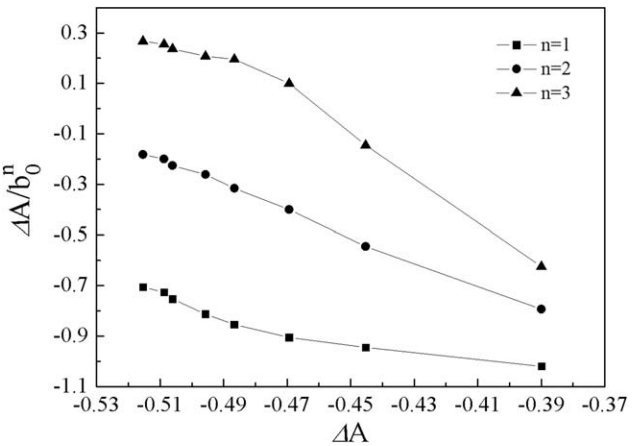

Figure 6. Plot of $\Delta A/{b_0}^n$ versus ΔA at 251 nm.

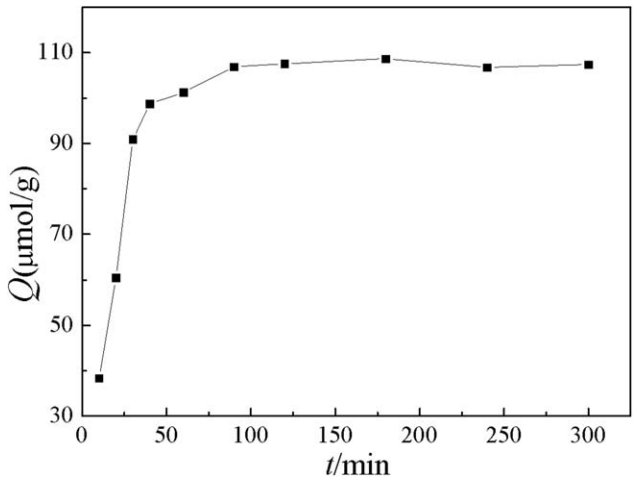

Figure 7. Adsorption kinetics of *p*-HB–SMIP.

To examine the underlying mechanism of the adsorption process, the kinetic data obtained were analyzed with the pseudo-first-order rate equation [eq. (13)] and pseudo-second-order rate equation [eq. (14)]:[31]

$$\log(Q_{\max} - Q_t) = \log Q_{\max} - \frac{k_1 t}{2.303} \tag{13}$$

$$\frac{t}{Q_t} = \frac{1}{k_2 Q_{\max}^2} + \frac{1}{Q_t} \tag{14}$$

where $Q_{\max}$ and Q_t are the adsorption capacities at equilibrium (μmol/g) and time t (μmol/g), respectively; t is the time (min); and k_1 and k_2 are the pseudo-first-order rate constant of adsorption (min^{-1}) and pseudo-second-order rate constant of adsorption (g $mmol^{-1}$·min^{-1}), respectively. The pseudo-first-order model rendered the rate of occupation of the adsorption sites to be proportional to the number of unoccupied sites, and the pseudo-second-order kinetic model was assumed to be the chemical reaction mechanisms and assumed that the adsorption rate was controlled by chemical adsorption through the sharing or exchange of electrons between the polymer and the adsorbent.

As shown in Table 1, the correlation coefficient for the pseudo-second-order model ($R^2 = 0.997$) was higher than that of the first-

Table 1. Kinetic Constants for the Pseudo-First-Order Equation and Pseudo-Second-Order Equation

Constants	Pseudo-first-order equation	Constants	Pseudo-second-order equation
[a]$Q_{e,c}$ (μmol/g)	22.07	[a]$Q_{e,c}$ (μmol/g)	112.5
[b]$Q_{e,max}$ (μmol/g)	109.1	[b]$Q_{e,max}$ (μmol/g)	109.1
k_1 (min^{-1})	0.0130	k_2(g/(mmol·min))	0.8840
R^2	0.5150	R^2	0.9970
[c]ΔQ (%)	390	[c]ΔQ (%)	3.01

[a] $Q_{e,c}$ is the theoretical calculating value of equilibrium adsorption capacity.
[b] $Q_{e,max}$ is the experimental value of equilibrium adsorption capacity.
[c] ΔQ (%) is the relative deviation between the theoretical and experimental equilibrium adsorption capacity.

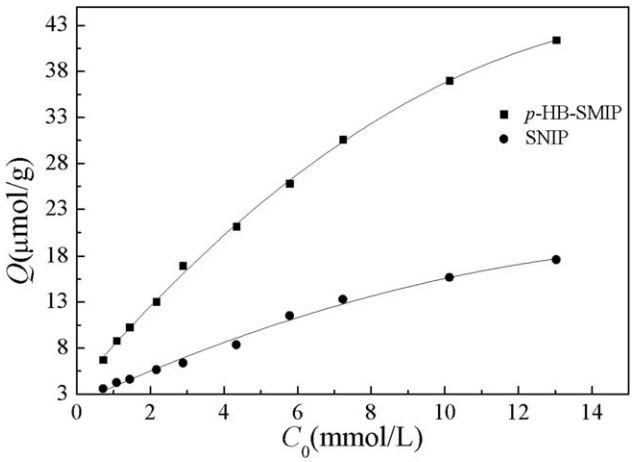

Figure 8. Adsorption isotherm curves of the *p*-HB–SMIP and SNIP at room temperature.

order model ($R^2 = 0.515$). Therefore, the adsorption behavior of *p*-HB on *p*-HB–SMIP belonged to the pseudo-second-order kinetic model, and the adsorption process was a chemical process.

Adsorption Isotherm

The adsorption isotherm of *p*-HB on *p*-HB–SMIP and SNIP was investigated at room temperature for 6 h, as shown in Figure 8. As shown in this figure, the equilibrium adsorption capacities of *p*-HB–SMIP and SNIP increased gradually with increasing concentration of *p*-HB in the initial solution and ultimately reached a stable value; the adsorption reached saturation. The difference in the adsorption amounts between *p*-HB–SMIP and SNIP got larger with increasing concentration of the template. *p*-HB–SMIP exhibited a higher adsorption capacity for *p*-HB than SNIP did at either a low or high concentration. These facts fully showed that the two kinds of polymer particles with almost the same elements were remarkably different in their space–structure; nonselective physical adsorption occurred between SNIP and *p*-HB. In contrast, the maximum adsorption capacity of *p*-HB–SMIP (41 μmol/g) toward *p*-HB was higher than that of SNIP (17 μmol/g). This suggested that *p*-HB–SMIP generated specific recognition sites in imprinting cavities.

Equilibrium data, commonly known as the *adsorption isotherm*, are basic requirements for designing adsorption systems. In this study, the equilibrium data for *p*-HB onto *p*-HB–SMIP and SNIP were modeled with the Langmuir, Freundlich, and Dubinin–Radushkevich isotherm models.[32–34] The applicability of the isotherm models to the adsorption behaviors was studied by judgment of the correlation coefficient. The adsorption isotherm constants for *p*-HB–SMIP and SNIP at 298 K are listed in Table II. Moreover, the comparison of the Langmuir, Freundlich, and Dubinin–Radushkevich isotherm models for *p*-HB adsorption onto *p*-HB–SMIP and SNIP with nonlinear regression are illustrated in Figure 9.

The Langmuir isotherm model assumes uniform adsorption on the surface and is used to describe monolayer adsorption on a surface containing a finite number of identical sites. The linear form is expressed by the following equation:

Table II. Adsorption Isotherm Constants for *p*-HB–SMIP and SNIP

Adsorption isotherm model	Parameter	*p*-HB-SMIP	SNIP
Freundlich equation	R^2	0.9950	0.9760
	K_F (μmol/g)	8.779	4.041
	n	1.582	1.742
Langmuir equation	R^2	0.9712	0.8812
	K_L (L/μmol)	0.1299	0.1597
	[a]$Q_{m,c}$ (μmol/g)	66.67	25.23
Dubinin–Radushkevich equation	R^2	0.7422	0.6114
	K_{DR} (mol^2/kJ^2)	0.0341	0.0229
	E (kJ/mol)	3.831	4.240

[a] $Q_{m,c}$ is the theoretical calculating value of maximum adsorption capacity.

$$\frac{C_e}{Q_e} = \frac{1}{Q_m K_L} + \frac{C_e}{Q_m} \tag{15}$$

where Q_e is the equilibrium adsorption capacity (μmol/g), Q_m is the maximum adsorption capacity of the sorbent, and K_L is the affinity constant.

The Freundlich adsorption isotherm is an empirical isotherm for nonideal adsorption on heterogeneous surfaces and multilayer adsorption. The Freundlich isotherm model as follows:

$$\log Q_e = \log K_F + (1/n)\ \log C_e \tag{16}$$

where K_F is an indicative constant for the adsorption capacity of the sorbent (μmol/g) and the constant $1/n$ indicates the intensity of the adsorption. A value of $n > 1.0$ represents a favorable adsorption condition.[35]

To further analyze the isotherms of the polymers with a high degree of rectangularity, we used the Dubinin–Radushkevich isotherm model. It is described as follows:

$$\ln Q_e = \ln Q_m - K_{DR}\,\varepsilon^2 \tag{17}$$

where ε is the Polanyi potential which can be determined from eq. (18):

$$\varepsilon = RT \ln [1 + (1/C_e)] \tag{18}$$

The constant K_{DR} is related to the free energy (E; kJ/mol) of adsorption per molecule of the adsorbate when it is transferred to the surface of the solid from infinity in the solution. It can be calculated by eq. (19):

$$E = (2K_{DR})^{-1/2} \tag{19}$$

where R is the gas constant (8.314 J mol^{-1} K^{-1}) and T is the absolute temperature. A plot of ln Q_e versus ε^2 enables the constants Q_m and E to be obtained.

From Table II, we concluded that the Freundlich isotherm model was more suitable for the experimental data than the

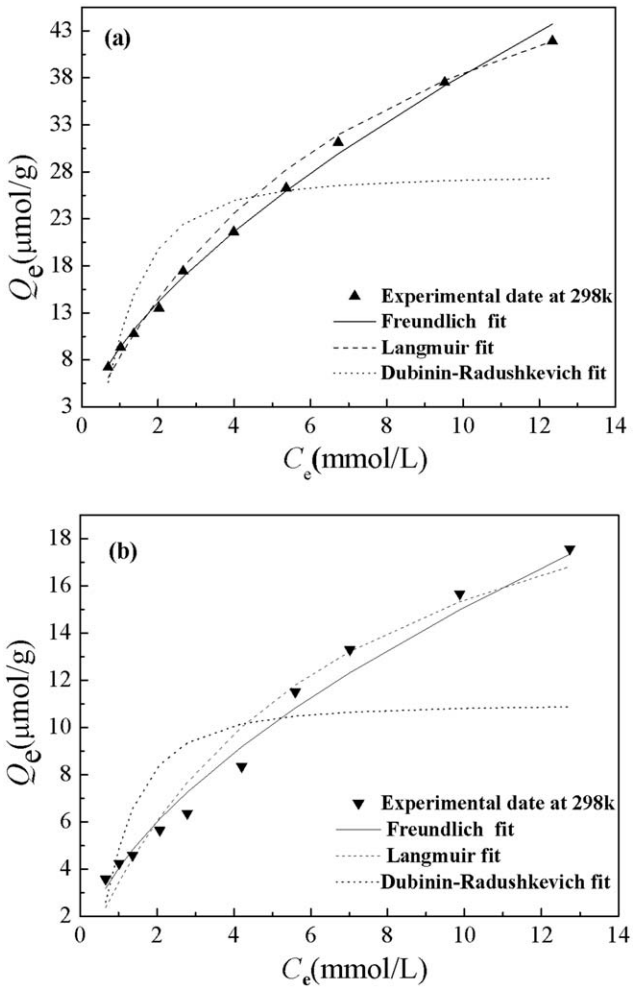

Figure 9. Comparison of the Langmuir, Freundlich, and Dubinin–Radushkevich isotherm models for *p*-HB adsorption onto (a) *p*-HB–SMIP and (b) SNIP with nonlinear regression.

Langmuir isotherm and Dubinin–Radushkevich isotherm. The values of the correlation coefficients for *p*-HB–SMIP ($R^2 = 0.995$) and SNIP ($R^2 = 0.976$) were higher than those calculated by the Langmuir model and Dubinin–Radushkevich equation and showed that the adsorption in this experiment obeyed the Freundlich model. The results show that the value of *n* was greater than unity; this indicated that *p*-HB was favorably adsorbed onto *p*-HB–SMIP and SNIP.

As shown in Figure 9, the nonlinear form of the Freundlich model also showed a better fit than the Langmuir model and Dubinin–Radushkevich equation for *p*-HB–SMIP and SNIP; this indicated a multimolecular layer adsorption for *p*-HB–SMIP and SNIP.

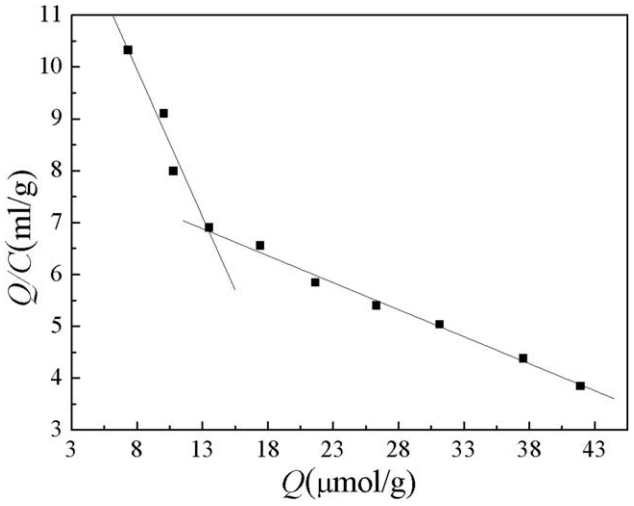

Figure 10. Scatchard curve for *p*-HB–SMIP.

Scatchard analysis was used to evaluate the binding affinity and the theoretical binding site number for the template of the molecularly imprinted material. Figure 10 shows the Scatchard plot of the adsorption of *p*-HB–SMIP for *p*-HB. As shown in this figure, there were two distinct linear sections within the plot. This suggested that there existed two types of binding sites with respect to the affinity for *p*-HB in the imprinted polymer particles; one was of high selectivity or affinity with a high binding energy, and the other was of low affinity with a low binding energy. From the slopes and intercepts of the two straight lines, the K_d and Q_{max} values were calculated, and the results are listed in Table III.

Adsorption Thermodynamics

Thermodynamic parameters, such as the changes in the Gibbs free energy (ΔG^o), enthalpy (ΔH^o), and entropy (ΔS^o), were calculated with the following equations:[35]

$$\ln\left(\frac{Q_e}{C_e}\right) = \frac{\Delta S^\circ}{R} - \frac{\Delta H^\circ}{RT} \quad (20)$$

$$\Delta G^o = \Delta H^o - T\Delta S^o \quad (21)$$

Thus, ΔH^o and ΔS^o were obtained from the slope and intercept of the line plotted by $\ln(Q_e/C_e)$ versus $1/T$, respectively. The obtained thermodynamic parameters for *p*-HB–SMIP and SNIP are listed in Table IV.

As illustrated in Table IV, a negative ΔG^o value indicated that the adsorption of *p*-HB–SMIP for *p*-HB was spontaneous within the temperature range evaluated; this is the case for many adsorption systems in solution. By abundant adsorption of *p*-HB onto the surface of *p*-HB–SMIP, the number of solvent molecules surrounding *p*-HB molecules decreased, and the

Table III. Results of the Scatchard Analysis

Binding site	Linear equation	K_d (μmol/mL)	Q_{max} (μmol/g)
Higher affinity site	$Q/C = 13.69 - 0.5660Q$ ($R^2 = 0.9431$)	1.770	24.19
Lower affinity site	$Q/C = 7.690 - 0.1040Q$ ($R^2 = 0.9872$)	9.620	73.94

Table IV. Thermodynamic Parameters for the Adsorption of *p*-HB onto *p*-HB–SMIP and SNIP

Polymer	ΔH^o (kJ/mol)	ΔS^o (J mol^{-1}. K^{-1})	ΔG^o (kJ/mol) 283 K	293 K	303 K
p-HB-SMIP	13.61	57.28	−2.600	−3.171	−3.751
SNIP	14.92	44.90	2.224	1.771	1.320

Table V. Adsorption Selectivity of *p*-HB–SMIP and SNIP

	p-HB-SMIP			SNIP	
	K_d (mL/g)	α	α′	K_d (mL/g)	α
p-HB	14.9			4.32	
p-ABA	5.36	2.79	2.82	4.30	0.99
BA	4.09	3.66	2.81	3.32	1.30
SA	2.48	6.03	4.79	3.41	1.26

degrees of the freedom of the solvent molecules increased. Therefore, the positive values of ΔS^o suggested increased randomness at the solid–solution interface during the adsorption of *p*-HB onto *p*-HB–SMIP.[36,37] In fact, the positive value of ΔH^o further confirmed the endothermic nature of the processes, so the increasing temperature caused more favorable adsorption of *p*-HB onto *p*-HB–SMIP.

Adsorption Selectivity

To investigate the selectivity of *p*-HB–SMIP, the adsorption capacities of *p*-HB–SMIP and SNIP in the mixed solution, including *p*-HB, SA, *p*-ABA, and BA, were examined by HPLC. The K_d, α, and α′ values are summarized in Table V. From the data in Table V, the following facts were found:

1. The K_d and α values of *p*-HB–SMIP presented a significant increase over than those of SNIP. This could be explained by the imprinting effect, abundant binding sites with functional groups in a predetermined orientation, and special size available for the selective recognition of *p*-HB onto *p*-HB–SMIP.
2. α′ is an indicator for expressing the adsorption affinity of recognition sites to the template molecules. The α′ results show that the selective recognition of *p*-HB–SMIP for *p*-HB were 2.82, 2.81, and 4.79 times greater than those of SNIP.
3. The α values of *p*-HB–SMIP for SA in relation to BA and *p*-ABA were greater. These results were attributed to the fact that the functional groups and molecular structure of BA and *p*-ABA were similar to those of *p*-HB. Therefore, the cavities imprinted by *p*-HB molecules on the surface of *p*-HB–SMIP were more suited to BA and *p*-ABA than to SA.

These results clearly reveal that *p*-HB–SMIP possessed high recognition and binding affinity for the *p*-HB molecules.

Catalytic Activity

The catalytic activities of *p*-HB–SMIP in the chlorination of toluene to *para*-chlorotoluene were investigated. The catalytic activities of *p*-HB–SMIP are illustrated in Table VI. As shown in Table VI, the products during the chlorination reaction were mainly *para*-chlorotoluene, *ortho*-chlorotoluene, benzyl chloride, and the little polychlorinated toluenes. It was clear that the values of conversion, the selectivity of the products, and the *p*/*o* values were all almost very low with no catalyst, especially for conversion (2.4%). However, the conversion of toluene greatly increased to 85.5, 72.4, and 36.8% with the addition of *p*-HB–SMIP, *p*-HB–NIP, and $FeCl_3$, respectively, as different catalysts. The *p*/*o* values for three different catalysts were on the order of *p*-HB–SMIP (1.38) > SNIP (0.62) > $FeCl_3$ (0.47). The imprinted polymer generally showed a higher catalytic activity for the chlorination of toluene to *para*-chlorotoluene compared to the nonimprinted polymer and traditional catalysts. These findings suggest that the effect of the cavity structures of *p*-HB–SMIP appeared on the binding step of the catalysis. This was because the template (*p*-HB) used here were product analogues, and the cavities imprinted with it had a complementary structure for the substrate (*para*-chlorotoluene) in the product state of the catalyzed reaction. Once the reactant was adsorbed on the surface of *p*-HB–SMIP and then entered into the cavities imprinted by *p*-HB molecules, the cavities displayed a catalytic effect on the generation of more *para*-chlorotoluene. The mechanism of the selective chlorination of toluene to *para*-chlorotoluene is shown in Figure 11.

Table VI. Chlorination of Toluene Catalyzed by Different Catalysts[a]

Catalysts	Conversion of Toluene (%)	Selectivity of products (%)[b]				*p*/*o* ratio [c]
		PCT	OCT	BC	others	
p-HB-SMIP	85.5	57.8	41.8	2.6	0.4	1.38
SNIP	72.4	38.7	56.5	4.7	0.2	0.62
$FeCl_3$	36.8	25.6	56.7	12.8	6.9	0.47
None	2.4	29.4	68.9	0.9	0.4	0.43

[a] Reaction conditions: catalyst = 0.5 g, Toluene = 10 ml, CH_3CN/Toluene (mol/mol) = 4:1, SO_2Cl_2 = 7.5 ml, reaction temperature = 60 °C, reaction time = 60 min.
[b] PCT = *para*-chlorotoluene, OCT = *ortho*-chlorotoluene; BC = benzyl chloride; Others = polychlorinated toluenes (di-, tri- and tetrachlorotoluenes).
[c] *o*/*p* = PCT/OCT.

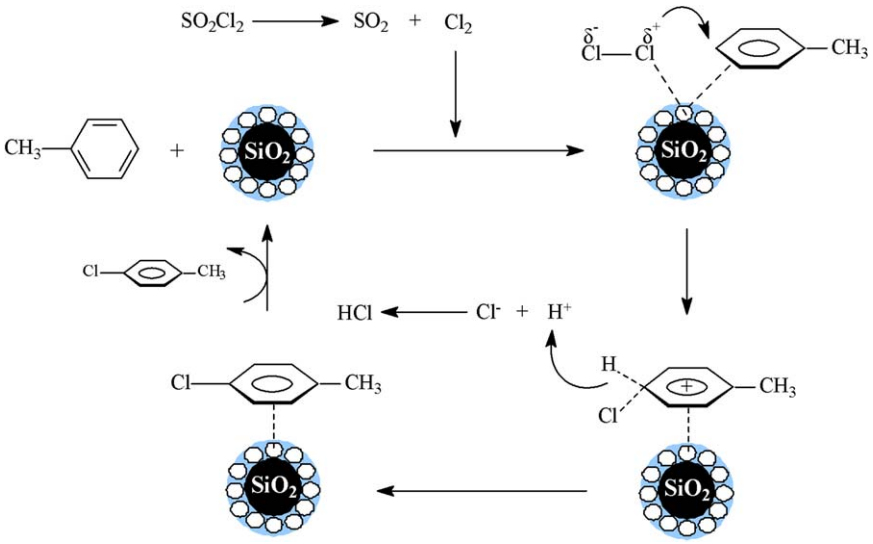

Figure 11. Mechanism of the chlorination of toluene. [Color figure can be viewed in the online issue, which is available at wileyonlinelibrary.com.]

CONCLUSIONS

In this investigation, the surface-imprinted technology was applied successfully to synthesize *p*-HB–SMIP for the selective catalysis of toluene to *para*-chlorotoluene for the first time. The characterization, kinetics, thermodynamics, selectivity, and regeneration were studied in detail. The adsorption isotherm studies indicated that the Freundlich model was more suitable for the adsorption of *p*-HB onto *p*-HB–SMIP than the Langmuir model or Dubinin–Radushkevich model. In addition, the kinetic study showed that the pseudo-second-order kinetic model fit very well with the dynamical adsorption behavior and implied that the adsorption behavior of *p*-HB on *p*-HB–SMIP was a chemical process. The values of ΔH^o, ΔG^o, and ΔS^o showed that the adsorption of *p*-HB on *p*-HB–SMIP was endothermic and spontaneous. The selectivity experimental results show that the *p*-HB–SMIP had excellent selectivity for the *p*-HB relative to the competition species. The catalytic activity investigation showed that *p*-HB–SMIP exhibited a higher catalytic activity and selectivity for the chlorination of toluene to *para*-chlorotoluene.

ACKNOWLEDGMENTS

This work was financially supported by the Ph.D. Innovation Programs Foundation of Jiangsu Province (contract grant number CXZZ13_0680). The authors thank Junjie Jing (Jiangsu University) very for his kindly support of the elemental analysis, UV–vis spectroscopy, and FTIR measurements of the samples.

REFERENCES

1. Hausladen, M. C.; Lund, C. R. F. *Appl. Catal. A* **2000**, *190*, 269.
2. Chang, C. C.; Burger, M. J.; Faitar, G. M.; Lund, C. R. F. *J. Catal.* **2001**, *202*, 59.
3. Wang, J. P.; Cormack, A. G.; Sherrington, D. C. *Angew. Chem. Int. Ed.* **2003**, *42*, 5336.
4. Wang, D. S.; Zhang, X. X.; Nie, S. Q.; Zhao, W. F.; Lu, Y.; Sun, S. D.; Zhao, C. S. *Langmuir* **2012**, *28*, 13284.
5. Meng, M. J.; Wang, Z. P.; Ma, L. L.; Zhang, M.; Wang, J.; Dai, X. H.; Yan, Y. S. *Ind. Eng. Chem. Res.* **2012**, *51*, 14915.
6. Jin, Y.; Jiang, M.; Shi, Y.; Lin, Y.; Peng, K.; Dai, B. *Anal. Chim. Acta* **2008**, *612*, 105.
7. Feng, Q. Z.; Zhao, L. X.; Yan, W.; Lin, J. M.; Zheng, Z. X. *J. Hazard. Mater.* **2009**, *167*, 282.
8. Haupt, K.; Mosbach, K. *Chem. Rev.* **2000**, *100*, 2495.
9. Holthoff, E. L.; Bright, F. V. *Acc. Chem. Res.* **2007**, *40*, 756.
10. Maier, N. M.; Lindner, W. *Anal. Bioanal. Chem.* **2007**, *389*, 377.
11. Ye, L.; Mosbach, K. *Chem. Mater.* **2008**, *20*, 859.
12. Cutivet, A.; Schembri, C.; Kovensky, J.; Haupt, K. *J. Am. Chem. Soc.* **2009**, *131*, 14699.
13. Bui, B. T. S.; Haupt, K. *Anal. Bioanal. Chem.* **2010**, *398*, 2481.
14. Hoshino, Y.; Koide, H.; Urakami, T.; Kanazawa, H.; Kodama, T.; Oku, N.; Shea, K. *J. Anal. Bioanal. Chem.* **2010**, *132*, 6644.
15. Urraca, J. L.; Aureliano, C. S. A.; Schillinger, E.; Esselmann, H.; Wiltfang, J.; Sellergren, B. *Anal. Bioanal. Chem.* **2011**, *133*, 9220.
16. Davis, M. E.; Katz, A.; Ahmad, W. R. *Chem. Mater.* **1996**, *8*, 1820.
17. Polborn, K.; Severin, K. *Chem. Eur. J.* **2000**, *6*, 4604.
18. Wulff, G. *Chem. Rev.* **2002**, *102*, 1.
19. Tada, M.; Iwasawa, Y. *J. Mol. Catal. A: Chem.* **2003**, *199*, 115.
20. Becker, J. J.; Gagne, M. R. *Acc. Chem. Res.* **2004**, *37*, 798.

21. Burri, E.; Ohm, M.; Daguenet, C.; Severin, K. *Chem. Eur. J.* **2005**, *11*, 5055.

22. Liu, J.; Wulff, G. *J. Am. Chem. Soc.* **2008**, *130*, 8044.

23. Wulff, G.; Liu, *J. Acc. Chem. Res.* **2012**, *45*, 239.

24. Resmini, M. *Anal. Bioanal. Chem.* **2012**, *402*, 3021.

25. Strikovsky, A. G.; Kasper, D.; Grün, M.; Green, B. S.; Hradil, J.; Wulff, G. *J. Am. Chem. Soc.* **2000**, *122*, 6295.

26. Svenson, J.; Zheng, N.; Nicholls, I. A. *J. Am. Chem. Soc.* **2004**, *126*, 8554.

27. Kalim, R.; Schomäcker, R.; Yüce, S.; Brüggemann, O. *Polym. Bull.* **2005**, *55*, 287.

28. Lu, Y.; Li, C. X.; Zhang, H. S.; Liu, X. H. *Anal. Chim. Acta* **2003**, *489*, 33.

29. Zhou, J.; He, X. W. *Anal. Chim. Acta* **1999**, *381*, 85.

30. He, J. F.; Zhu, Q. H.; Deng, Q. Y. *Spectrochim. Acta A* **2007**, *67*, 1297.

31. Meng, M. J.; Feng, Y. H.; Zhang, M.; Liu, Y.; Ji, Y. J.; Wang, J.; Wu, Y. L.; Yan, Y. S. *Chem. Eng. J.* **2013**, *225*, 331.

32. Allen, S. J.; Mckay, G.; Porter, J. F. *J. Colloid Interface Sci.* **2004**, *280*, 322.

33. Mazzotti, M. *J. Chromatogr. A* **2006**, *1126*, 311.

34. Terzyk, A. P.; Wojsz, R.; Rychlicki, G.; Gauden, P. A. *Colloids Surf. A* **1996**, *119*, 175.

35. Li, K. Q.; Wang, X. H. *Bioresour. Technol.* **2009**, *100*, 2810.

36. Mellah, A.; Chegrouche, S.; Barkat, M. *J. Colloid Interface Sci.* **2006**, *296*, 434.

37. Wu, J.; Yu, H. Q. *J. Hazard. Mater.* **2006**, *137*, 498.